Dynamic Fluence Modulation using Proton CT for Low-dose Imaging in Particle Therapy

Jannis Dickmann, Christina Sarosiek, George Coutrakon, Simon Rit, Nick Detrich, Victor Rykalin, Mark Pankuch, Robert P. Johnson, Reinhard Schulte, Katia Parodi, et al.

Dynamic Fluence Modulation using Proton CT for Low–dose Imaging in Particle Therapy

Jannis Dickmann, Christina Sarosiek, George Coutrakon, Simon Rit, Nick Detrich, Victor Rykalin, Mark Pankuch, Robert P. Johnson, Reinhard W. Schulte, Katia Parodi, Guillaume Landry, and George Dedes

***Abstract*—Dynamic fluence modulation for computed tomography (CT), i.e. the acquisition of tomographic images with variable, patient- and task-specific fluence fields, offers the potential to substantially reduce local imaging dose. In particular, volume-of-interest (VOI) imaging allows to limit imaging dose to a clinically relevant volume and reduce it elsewhere. In the context of particle therapy, where tomographic data is required for treatment planning the VOI is the treatment beam path. VOI imaging is of particular interest for particle therapy given the very low integral out-of-VOI treatment dose. Proton CT imaging allows for a direct measurement of the proton stopping power with an increased accuracy and a decreased imaging dose compared to x-ray-based CT. In addition, frequent imaging is required to verify patient positioning and to monitor potential anatomical changes, which over the course of a treatment may compromise the planned dose. In this work, we evaluate the performance of a fluence-modulated proton CT algorithm for low-dose in-room imaging. This would allow for recalculation or replanning of the treatment dose according to the anatomy of the day with out-of-VOI dose below 1 mGy. We performed a simulation study and acquired experimental data using a prototype proton CT scanner. By employing a bow-tie-like fluence modulation aiming for constant noise, imaging dose was reduced by 9%. For a VOI imaging task, out-of-VOI dose was reduced by 41% and substantially below 1 mGy. This may pave the way for daily imaging prior to every treatment session aiming to eventually reduce safety margins in particle therapy, thus further reducing normal tissue exposure to therapeutic doses.**

I. Introduction

IMAGE-GUIDED particle therapy requires an accurate volumetric representation of the proton (or heavier ion) stopping power for calculation and optimization of the therapeutic dose. Ideally, images are acquired at minimal imaging dose prior to each treatment fraction and in treatment position to avoid suboptimal tumor coverage due to positioning errors or anatomical changes. The current clinical practice is to use single or (less frequently) dual energy x-ray computed tomography (xCT) and a subsequent calibration mapping photon attenuation to the relative (to water) stopping power (RSP). This procedure leads to intrinsic errors of approx. 1% (dual energy) to 3% (single energy) in RSP [1]. To account for such uncertainties, additional safety margins are added to the planning target volume, which necessarily results in a higher dose delivered to healthy tissue or even organs-at-risk during treatment. Furthermore, dual energy xCT imaging, when available, cannot be easily performed in treatment position, and, due to timing and imaging dose constraints, is not performed prior to every treatment fraction at most centers.

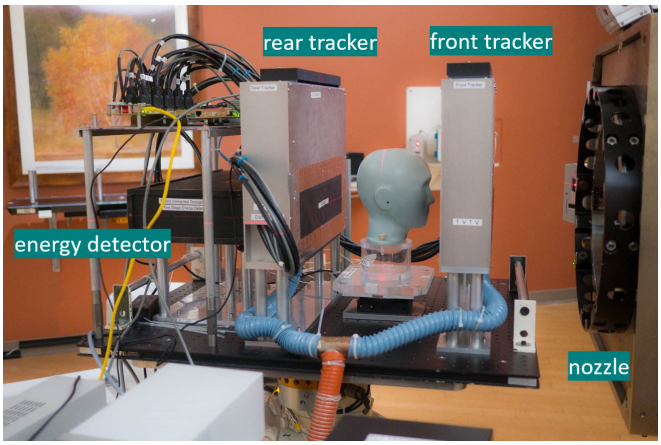

Fig. 1. Prototype proton CT scanner mounted on top of a robotic arm in front of the treatment beam nozzle. Two tracking detectors measure positions and directions of each proton and an energy detector measures its residual energy.

Alternatively, a direct determination of the RSP is possible using proton computed tomography (pCT) by measuring the energy loss of high-energy (e.g. 200 MeV for cranial indications) protons traversing the patient, as originally proposed by Cormack [2]. The energy loss of a single proton is directly linked to a line integral through RSP, which can therefore be reconstructed using iterative or analytical image reconstruction accounting for the curved path of the protons [3]. RSP accuracy of images acquired using the pre-clinical prototype pCT scanner [4], [5] shown in fig. 1 is reported to be competitive to state-of-the-art dual energy xCT with optimal spectral separation [6]. At the same time, future pCT scanners could readily be rotated with the proton gantry and images be

J. Dickmann, Prof. Dr. K. Parodi, Prof. Dr. G. Landry, and Dr. G. Dedes are with the Ludwig-Maximilians-Universität München (LMU Munich), Germany. Prof. Dr. G. Landry is also with the University Hospital, LMU Munich, Germany and the German Cancer Consortium (DKTK), Munich, Germany. C. Sarosiek and Prof. Dr. G. Coutrakon are with the Northern Illinois University, USA. Dr. S. Rit is with CREATIS and University of Lyon, France. N. Detrich. Dr. V. Rykalin and Dr. M. Pankuch are with the Northwestern Medicine Chicago Proton Center, USA. N. Detrich is also with IBA, Louvain-La-Neuve, Belgium. Dr. V. Rykalin is also with Proton VDA Inc., Naperville, USA. Prof. Dr. R. P. Johnson is with University of California, Santa Cruz, USA. Prof. Dr. R. W. Schulte is with Loma Linda University, USA.

Corresponding author: jannis.dickmann@lmu.de.

acquired in treatment position just before treatment. Moreover, dose efficiency is improved compared to xCT [7] and typical pCT imaging doses are at 1 to 2 mGy per tomography and therefore at the level of cone-beam xCT, yet with the dosimetric accuracy of dual energy xCT. The rate of double-strand DNA breaks by pCT may also be reduced compared to xCT at equivalent physical dose [8], [9]. This makes pCT a good candidate for frequent pre-treatment recalculation and optional replanning of the therapeutic dose, without accumulation of critical imaging doses.

A further reduction of imaging dose can be achieved by using dynamic fluence field modulation, originally proposed for xCT [10], [11]. Fluence-modulated imaging aims at inhomogeneous and changing spatial distributions of radiation fluence within one projection, thus concentrating imaging dose within a volume-of-interest (VOI), where image noise is low. Elsewhere, image noise is elevated, but imaging dose reduced. This is particularly meaningful in the context of particle therapy, where low noise (and high RSP accuracy) is only required within the treatment beam path (i.e. the VOI) and image noise (and RSP accuracy) is irrelevant elsewhere. At the same time, imaging dose outside the VOI must be kept low to maintain the low dose to normal tissue achievable with proton therapy – and is irrelevant inside the VOI, where therapeutic dose dominates. While experimental implementation of fluence modulation in xCT is challenging [12], [13], the incident proton fluence can readily be modulated by scanning the object with proton pencil beams using the treatment beam delivery system and modulating the dwell time or beam current of each pencil beam. The typical size of a proton pencil beam is about 10 mm (FWHM), which allows for a fine modulation of the fluence.

In this work, we evaluate a previously presented optimization algorithm for fluence-modulated pCT (FMpCT) [14] for its ability to reduce imaging dose and achieve prescribed image noise distributions. We employ both a Monte Carlo simulation of the imaging set-up and experimental data.

II. Materials & Methods

A. Image noise for proton CT

The pCT prototype scanner investigated in this work records position, direction and residual energy information for every proton incident to the detector – an operation mode called "list-mode." Variance in list-mode pCT projections is proportional to the number of particles per pixel in the projection (referred to as "counts"), because the projection value is the average water-equivalent path length (WEPL) of a set of protons incident to each pixel. For a given number of counts, noise is primarily affected by the protons' stochastic loss of energy, known as "energy straggling," in the object and also in the detector. Moreover, multiple Coulomb scattering (MCS) of protons and the accuracy of the proton path estimate through tracking impact noise. Finally, the energy spread of the accelerator can increase noise. All these contributions were quantified in a previous publication [15] and can be predicted precisely using a Monte Carlo simulation of the prototype pCT scanner shown in fig. 1 and used in this study. It is important to note that MCS is object-dependent and heterogeneities strongly increase noise, distorting the bijective relation between line integral values and noise levels which can be expected in xCT. Therefore, any fluence modulation must take into account prior knowledge about the object to be imaged, for example from a previous diagnostic xCT or pCT scan, or even MRI converted to xCT [16]. Given noise levels in the projection, image noise can be calculated using variance reconstruction [17], [18], which is an error propagation through the linear reconstruction operation of filtered backprojection.

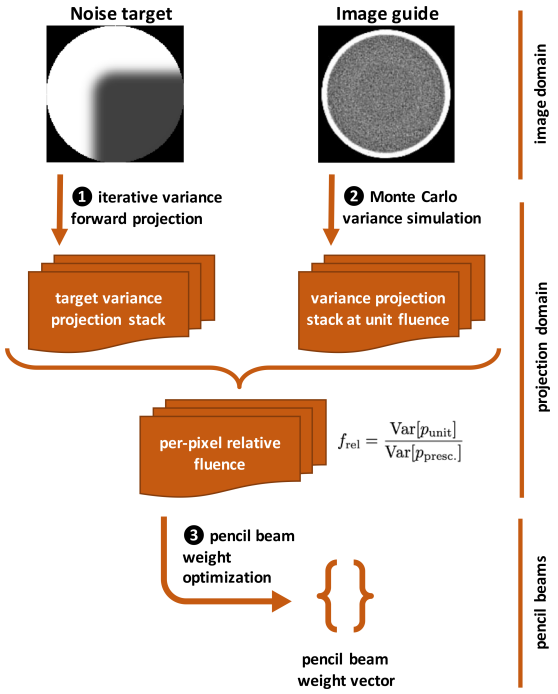

Fig. 2. Three-step projection-based optimization workflow for fluence-modulated pCT: given an image noise target and an image guide, the algorithm calculates a pencil beam weight vector that results in the desired image noise target for a given object.

B. Fluence optimization algorithm

The fluence-modulation optimization algorithm presented in [14] calculates a set of pencil beam weights (i.e. their relative dwell time) that achieve a prescribed image noise target. The workflow is depicted in fig. 2 and consists of three steps.

At first, an iterative variance forward projection is employed, that finds a strictly positive (and thus physical) stack of variance projections $\mathrm{Var}[p_{\mathrm{presc.}}]$, resulting in the prescribed image noise target when input to the variance reconstruction.

In a second step, a Monte Carlo simulation is used to generate a set of variance projections $\mathrm{Var}[p_{\mathrm{unit}}]$, which correspond to imaging the object at some unit fluence (e.g. uniform fluence). This incorporates prior knowledge about the object to be imaged. Since variance is inversely proportional to the number of counts, the required fluence modulation (relative to unit fluence) is calculated as $f_{\mathrm{rel}} = \mathrm{Var}[p_{\mathrm{unit}}] / \mathrm{Var}[p_{\mathrm{presc.}}]$, which would already be sufficient if it were possible to modulate fluence pixel-by-pixel.

A third step therefore includes knowledge about the finite extent of each pencil beam. A linear combination of a set of pre-

defined pencil beams is calculated, such that the summed fluence is equal to

$$F_{\mathrm{FMpCT}} = F_{\mathrm{unit}} \cdot f_{\mathrm{rel}} = F_{\mathrm{unit}} \cdot \mathrm{Var}[p_{\mathrm{unit}}] / \mathrm{Var}[p_{\mathrm{presc.}}], \quad (1)$$

where F_{unit} is the unit fluence of all pencil beams. This optimization problem is solved by minimizing the summed squared pixel-wise deviation between eq. (1) and a linear combination of pencil beams. The pencil beam model for this optimization (spot size, divergence) was derived from experimental data. Pencil beam centers were chosen to be on a regular grid as shown in the last row of fig. 3 (a). The large spacing in horizontal direction was compensated by shifting the fluence pattern by a quarter of this spacing, resulting in a homogeneous fluence when summing counts of two opposing projections (analogous to the quarter detector shift in xCT).

C. *Simulation study*

A Monte Carlo simulation study was performed using a dedicated Geant4 simulation platform [19], which we recently validated for its accuracy in predicting RSP noise [15]. A water filled cylindrical PMMA container (diameter 150.5 mm) was simulated, for which a physical counterpart existed. Three scenarios were investigated: (1) acquisition with uniform fluence (i.e. unit fluence), which is current standard for pCT acquisitions; (2) prescription of constant noise throughout the water cylinder; and (3) an FMpCT acquisition with a VOI in one quadrant mimicking the beam path of a two-field treatment with therapeutic beams from 90 and 180 degrees. Fluence patterns were optimized using the algorithm in section II.B. Imaging doses were scored for every projection and summed.

D. *Experimental acquisitions*

Experimental data were acquired using the pCT prototype scanner [4] shown in fig. 1 and located at a fixed beam line of the Northwestern Medicine Chicago Proton Center, which is capable of pencil beam scanning. The object was rotated for a full 360 degrees during the acquisition. An interface to the

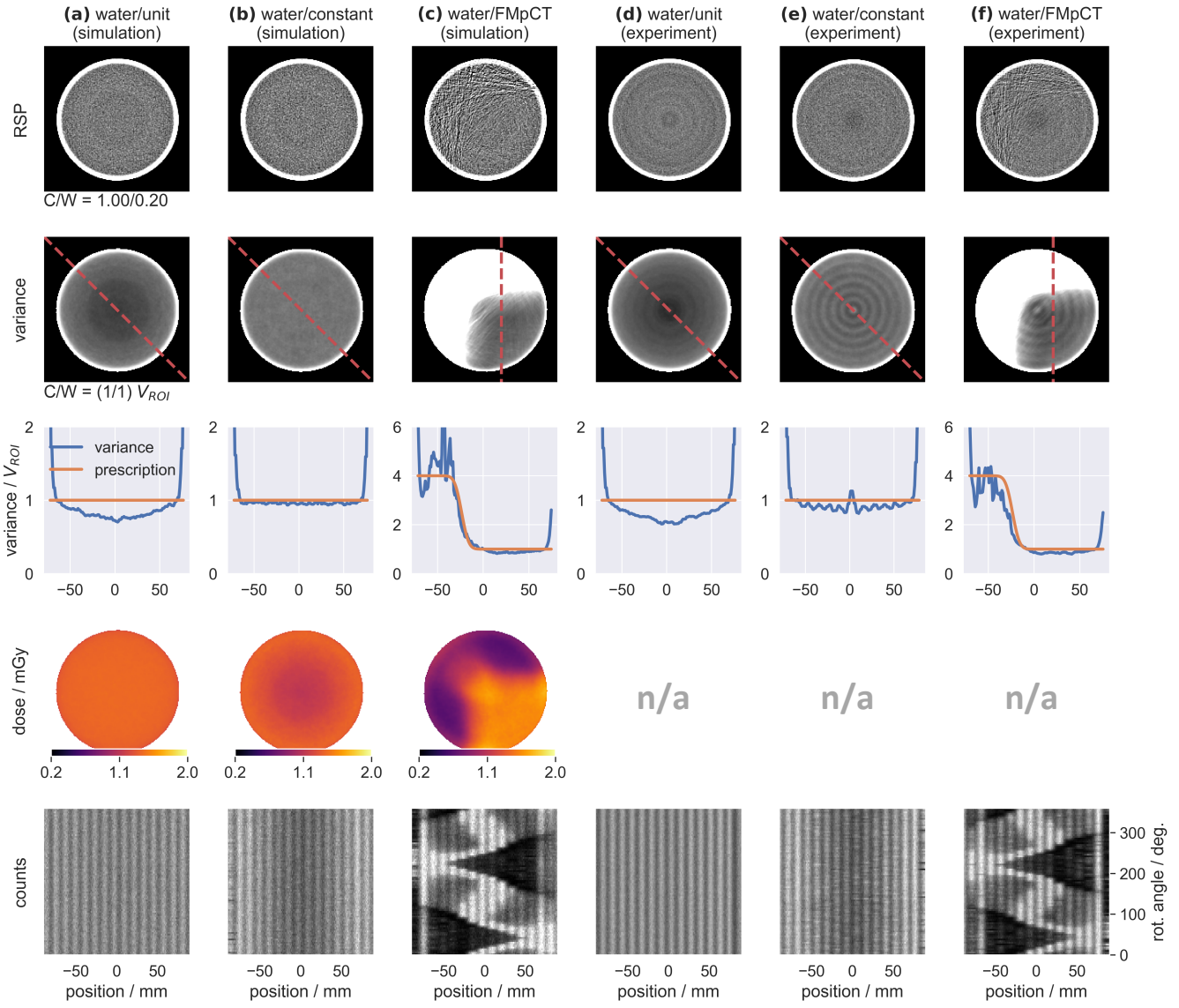

Fig. 3. Simulation (a, b, c) and experimental (d, e, f) pCT acquisitions for unit fluence (a, d), a constant noise (b, e) and an FMpCT noise prescription (c, f). RSP, variance, simulated imaging dose and counts sinograms are displayed.

beam control system was developed to automatically deliver fluence patterns. The same water filled phantom as in the simulation study was used. Noise targets and optimized fluence patterns were also identical.

III. Results & Discussion

Results are summarized in fig. 3, where RSP maps, the variance reconstruction, profiles through the variance reconstruction (indicated by the dashed line), imaging doses and counts sinograms are shown. Simulation study results are in fig. 3 (a) to (c) and experimental results in fig. 3 (d) to (f).

In fig. 3 (a) unit fluence was delivered as can be seen in the counts sinogram. This resulted in a reduced image variance in the center of the object, which is expected due to multiple Coulomb scattering and was discussed in a previous publication [15]. Imaging dose is constant throughout the object because the energy loss for high energy protons (far from the Bragg peak) is relatively constant. Fig. 3 (b) shows an optimized fluence plan aiming for constant variance in the image, which was successful as can be seen in the variance map and profile. While the change in the RSP image is not directly obvious, the counts sinogram shows reduced fluence in the center of the object, which at the same place resulted in a reduced dose. This is the equivalent of a bow-tie filter in xCT, but the fluence profile is fundamentally different due to different noise characteristics in pCT. At equal peak noise level, dose was reduced by 9% using fluence modulation, compared to the unit fluence scan. The effect of the FMpCT plan in fig. 3 (c) can already be appreciated in the RSP map. The variance map and profile show that fluence modulation was successful and variance follows the prescription with good accuracy. At equal peak noise level in the VOI, dose outside of the VOI was reduced by 41%, which is a substantial dose saving. In [14], an anthropomorphic head phantom was also studied showing similar dose savings for a more heterogeneous geometry.

Experimental data in fig. 3 (d) to (f) agree well with results from the simulation study. Unfortunately, the alignment of the scanner with respect to the coordinate system of the beam line was not perfectly reproduced in between the unit fluence acquisition and the two fluence modulations. This caused the quarter shift of the pencil beam pattern to be spoiled and resulted in rings in the variance map due to changing proton statistics. Except for this minor disagreement, the variance maps using fluence modulation were as expected from simulations. While variance rings partially impaired the constant noise target in fig. 3 (e), the FMpCT acquisition in fig. 3 (f) agreed well with the prescription, and the prescribed variance difference was larger than the ringing caused by the misalignment. Imaging doses were not determined for the experimental dataset, but dose savings can be expected to be comparable to those determined in the simulation study, especially given that fluence sinograms were very similar.

IV. Conclusion

In this work, we generated fluence-modulated pCT delivery patterns using a dedicated optimization algorithm for FMpCT. Patterns were calculated for a simple water-filled cylinder and for two noise prescriptions: constant noise throughout the image as an equivalent to xCT bow-tie filters, and a volume-of-interest imaging task with application for particle therapy. The performance of the optimization algorithm was evaluated both in a simulation study and in an experiment using a prototype pCT scanner. Dose savings in the simulation study were substantial, highlighting the potential use of fluence modulation in pCT. Experimental feasibility was demonstrated but leaves room for technical improvements not related to the optimization algorithm.

Acknowledgment

This work was supported by the German Research Foundation (DFG) under grant #388731804. Additional support from the Munich-Centre for Advanced Photonics, the Bavaria-California Technology Center and the Franco-Bavarian university cooperation center is gratefully acknowledged.

References

[1] H. Paganetti, “Range uncertainties in proton therapy and the role of Monte Carlo simulations,” *Phys. Med. Biol.*, 57, 11, R99–R117, 2012.
[2] A. M. Cormack, “Representation of a Function by Its Line Integrals, with Some Radiological Applications,” *J. Appl. Phys.*, 34, 9, 2722–2727, 1963.
[3] S. Rit *et al.*, “Filtered backprojection proton CT reconstruction along most likely paths,” *Med. Phys.*, 40, 3, 031103, 2013.
[4] R. P. Johnson *et al.*, “A Fast Experimental Scanner for Proton CT: Technical Performance and First Experience With Phantom Scans,” *IEEE Trans. Nucl. Sci.*, 63, 1, 52–60, 2016.
[5] V. A. Bashkirov *et al.*, “Novel scintillation detector design and performance for proton radiography and computed tomography,” *Med. Phys.*, 43, 2, 664–674, 2016.
[6] G. Dedes *et al.*, “Experimental comparison of proton CT and dual energy x-ray CT for relative stopping power estimation in proton therapy,” *Phys. Med. Biol.*, 64, 16, 165002, 2019.
[7] R. W. Schulte *et al.*, “Density resolution of proton computed tomography,” *Med. Phys.*, 32, 4, 1035–1046, 2005.
[8] S. Meyer *et al.*, “Dosimetric accuracy and radiobiological implications of ion computed tomography for proton therapy treatment planning,” *Phys. Med. Biol.*, 2019.
[9] L. Yasui *et al.*, “DNA Double-Strand Break Induction and Repair of Proton Computed Tomography in Normal Human Cells,” in *RSNA Annual Meeting*, 2019.
[10] S. A. Graham *et al.*, “Intensity-modulated fluence patterns for task-specific imaging in cone-beam CT,” in *Proceedings of SPIE*, 2007, 651003.
[11] S. Bartolac *et al.*, “Fluence field optimization for noise and dose objectives in CT,” *Med. Phys.*, 38, 7, S2–S17, 2011.
[12] J. W. Stayman *et al.*, “Fluence-field modulated x-ray CT using multiple aperture devices,” *Proceedings of SPIE*, 9783, 97830X, 2016.
[13] S. Huck *et al.*, “Optimized intensity modulation for a dynamic beam attenuator in x-ray computed tomography,” in *Proceedings of SPIE*, 2019, 1094824, p. 75.
[14] J. Dickmann *et al.*, “An optimization algorithm for dose reduction with fluence-modulated proton CT,” *Med. Phys.*, 47, 4, 1895–1906, 2020.
[15] J. Dickmann *et al.*, “Prediction of image noise contributions in proton computed tomography and comparison to measurements,” *Phys. Med. Biol.*, 64, 14, 145016, 2019.
[16] S. Neppl *et al.*, “Evaluation of proton and photon dose distributions recalculated on 2D and 3D Unet-generated pseudoCTs from T1-weighted MR head scans,” *Acta Oncol.*, 58, 10, 1429–1434, 2019.
[17] A. Wunderlich and F. Noo, “Image covariance and lesion detectability in direct fan-beam x-ray computed tomography,” *Phys. Med. Biol.*, 53, 10, 2471–2493, 2008.
[18] M. Rädler *et al.*, “Two-dimensional noise reconstruction in proton computed tomography using distance-driven filtered back-projection of simulated projections,” *Phys. Med. Biol.*, 63, 21, 215009, 2018.
[19] V. Giacometti *et al.*, “Software platform for simulation of a prototype proton CT scanner,” *Med. Phys.*, 44, 3, 1002–1016, 2017.